Enhancement of full-spectrum photocatalytic activity over $BiPO_4/Bi_2WO_6$ composites

Yanyan Zhu[a, b ‡], Yajun Wang[c ‡], Qiang Ling[b] and Yongfa Zhu[a,*]

[a] Department of Chemistry, Beijing Key Laboratory for Analytical Methods and Instrumentation, Tsinghua University, Beijing 100084, P.R. China;

[b] Institute of Aeronautical Meteorology and Chemical Defence, Beijing 100085, P.R. China;

[c] State Key Laboratory of Heavy Oil Processing, China University of Petroleum, Beijing 102249, China

Abstract: The full-spectrum photocatalytst is of important value for the practical use, which could absorb natural sunlight for photoctalytic degrading organic pollutants. $BiPO_4/Bi_2WO_6$ composite photocatalysts were prepared via ultrasonic-calcination method and had superior photocatalytic performance for degrading different kinds of organic pollutants under simulant sunlight irradiation. The apparent rate constant of 5.0%$BiPO_4/Bi_2WO_6$ on the degradation of methylene blue (MB) is 0.0305 min^{-1}, which is about 25.4 and 3.2 times of pure $BiPO_4$ and Bi_2WO_6 respectively. In the $BiPO_4/Bi_2WO_6$ composite photocatalysts, the core-hole structure of $BiPO_4$ as core and Bi_2WO_6 as hole was formed. During the photocatalytic process of $BiPO_4/Bi_2WO_6$ composites under simulant sunlight irradiation, the photo-generated electrons of $BiPO_4$ would inject to the conduction band of Bi_2WO_6, and the photo-generated holes on Bi_2WO_6 could transfer to the valance band of $BiPO_4$, and then an effective charges separation was achieved. The interaction of $BiPO_4$ and Bi_2WO_6 not only expanded the range of absorption spectrum but also enhanced the separation efficiency of photo-generated charges, and further improved the photocatalytic performance.

Keywords: $BiPO_4/Bi_2WO_6$ composites; Full-spectrum; Photocatalytic degradation

1. Introduction

Photocatalysis has an important value in environmental purification and energy use utilization in recent years. The study of full-spectrum photocatalyst is the key technology that makes the best use of natural sunlight to purify environment [1, 2]. Recently, much attention has been given to Bi-based photocatalysts [3]. As a visible photocatalyst, Bi_2WO_6 possesses many advantages such as high activity, stable property and so on, which ascribes to the structure that the octahedron of ceratoid WO_6 locates in the sandwich of $(Bi_2O_2)^{2+}$ and promote the quick separation of photo-generated charges. Bi_2WO_6 has attracted more attention on the photocatalytic degradation of organic pollutants, however it still need further improve the photocatalytic efficiency in practical use [4-7]. Bi_2WO_6 doped with noble metal cocatalyst such as Au[8], Ag[9, 10], Pt[11] or composited other semiconductor photocatalysts such as TiO_2[12, 13], ZnO[14], AgBr[15], Ag_3PO_4[16], $BiVO_4$[17], Bi_2O_3[18] and Co_3O_4[19], C_3N_4[20, 21] to further improve photoctatalytic performance. $BiPO_4$, as a high active ultraviolent photocatalyst, has been attached importance by more and more researchers recently. Our research groups prepared three kinds of crystal structure and different morphology $BiPO_4$ photocatalysts via various methods such as hydrothermal, solvothermal, reflux and calcination, the photocatalytic activity of monazite monoclinic $BiPO_4$ is much better than that of traditional P25 TiO_2[22-26]. Because the band gap of $BiPO_4$ is very wide, which only is excited by ultraviolent under 300 nm wavelength. In order to expand the absorption range and improve the photocatalytic activity, $BiPO_4$ was composited with RGO[27], C_3N_4[28, 29], BiOI[30, 31], BiOBr[32, 33], Ag_3PO_4[34-36], Bi_2MoO_6[37], $BiVO_4$[38], AgBr[39], AgI[40] and so on.

Based on merits and shortcomings of $BiPO_4$ and Bi_2WO_6 photocatalysts, $BiPO_4/Bi_2WO_6$ composites were prepared via ultrasonic-calcination method in this work. Under the simulant sunlight irradiation, the photocatalytic activity of $BiPO_4/Bi_2WO_6$ on the degradation of different kinds of organic pollutants was evaluated. Moreover, physicochemical properties and the proposed enhancement mechanism of $BiPO_4/Bi_2WO_6$ photocatalytic activity were also systematically investigated.

2. Experimental Section

2.1 Synthesis of $BiPO_4/Bi_2WO_6$ composite photocatalysts

Monazite monoclinic $BiPO_4$ nanorods prepared via reflux was used as precursor[25]. Appropriate amount $BiPO_4$ was weighed and added into a beaker, then 4.85 g (10 mmol)

$Bi(NO_3)_3 \cdot 5H_2O$ and 3.3 g (10 mmol) $Na_2WO_6 \cdot 2H_2O$ were added as 1:1 mole ratio, at last 900 ml deionized water was added. The mixture was ultrasonicated for 1.0 h and then vigorously stirred for 1.0 h. A white precipitate was obtained by centrifugation and washed with deionized water for 3 times. Finally, the product was dried at 120 °C for 12.0 h and then calcinated in the muffle furnace in air at 500 °C for 4.0 h. According to the addition amount of $BiPO_4$, 0.5%, 1.0%, 3.0%, 5.0%, 8.0% and 10.0%$BiPO_4/Bi_2WO_6$ composite photocatalysts were obtained respectively.

2.2 Evaluation of Photocatalytic Activity and Photoelectrochemical Performance

The photocatalytic activity of as-prepared $BiPO_4/Bi_2WO_6$ composite photocatalysts were evaluated by degradation of MB in aqueous solution under a 500 W simulant sunlight xenon lamp irradiation (Institute for Electric Light Sources, Beijing) with no or different wavelength band-pass filter. 25 mg photocatalyst was added into as-prepared 50 mL 1.0×10^{-5} $mol\cdot L^{-1}$ MB aqueous solution. Before irradiation, the suspension was ultrasonically dispersed for 0.5 h and then magnetically stirred for 1.0 h in dark to ensure the establishment of adsorption−desorption equilibrium. At each given time intervals, 3.0 mL suspension was taken out and separated through centrifugation (4000 rpm, 10 min). The concentration of MB solution was analyzed at the absorption band maximum (663 nm) using a Hitachi U-3010 UV-Vis spectrophotometer. The methods for the photocatalytic degradation of methyl orange (MO), Rhodamine B (RhB) and phenol were the same as above, but the concentration of phenol was 5.0 $mg\cdot L^{-1}$. The concentration of phenol is monitored using HPLC analysis with a UV detector at 270 nm. The mobile phase was methanol and water as 6:4, and the flow rate was 1.0 $mL\cdot min^{-1}$.

The photocurrents and electrochemical impedance spectroscopy (EIS) of $BiPO_4/Bi_2WO_6$ photocatalysts were performed on CHI-660B electrochemical system (Shanghai, China) using a standard three-electrode cell under simulant sunlight irradiation. The ITO/samples with 20 mm×45 mm was acted as a working electrode, a standard calomel electrode (SCE) was used as reference electrode and a platinum wire was used as the counter electrode. ITO/$BiPO_4/Bi_2WO_6$ was prepared by a dip−coating method: 6 mg $BiPO_4/Bi_2WO_6$ photocatalyst was suspended into 0.75 mL ethanol to make slurry, which was then dip−coated onto ITO glass electrode. The as−prepared electrodes were dried under ambient conditions for about 12.0 h and then calcinated at 120 °C for 5.0 h in air. Unless otherwise stated, the intensity of light at the film electrode was 1.5 $mW\cdot cm^{-2}$ and 0.1 $mol\cdot L^{-1}$ Na_2SO_4 electrolytes were used. The photoelectric responses of the sample as light-on and light-off were measured

at 0.0 V. The electrochemical impedance spectroscopy (EIS) was carried out at the open circuit potential, and a sinusoidal ac perturbation of 5 mV was applied to the electrode over the frequency range of 0.05-10^5 Hz.

2.3 Materials Characterization

The crystallinity and purity of $BiPO_4/Bi_2WO_6$ samples were characterized by X-ray diffraction (XRD) on a Bruker D8 Advance diffractometer (Cu Kα=1.5418 Å, tube voltage=40 kV, tube current=20 mA) at a scan rate of $2°\cdot min^{-1}$ in the 2θ range from 10° to 65°. The Ultraviolet−Visible diffuse reflectance spectroscopy (UV−Vis DRS) of $BiPO_4/Bi_2WO_6$ photocatalysts were performed on Hitachi U-3010 spectrophotometer equipped with an integrated sphere attachment in the range of 200 to 800 nm, and $BaSO_4$ was used as reference. The particle sizes of $BiPO_4/Bi_2WO_6$ samples were measured on the HITACHI HT7700 transmission electron microscopy (TEM) with an accelerating voltage 100 kV. The EDS mapping and the lattice planes and fringes of $BiPO_4/Bi_2WO_6$ were obtained from the high-resolution transmission electron microscope (HRTEM, JEM 2010F), and it was operated at an accelerating voltage of 200 kV. The Raman spectrum was measured at room temperature using HORIBAR 800 microscopic confocal Raman spectrometer in the range of 2000 cm^{-1} to 4000 cm^{-1}, and the excitation wavelength was the 514.5 nm from an Ar^+ laser with 30 mW output power. The electron spin resonance (ESR) signals of radicals spin-trapped by spin-trap reagent 5,5′-dimethyl-1-pirroline-N-oxide(DMPO) were examined on a Bruker model ESR JES-FA200 spectrometer equipped with a Quanta-Ray Nd:YAG laser system as the irradiation source (λ = 365 nm). Magnetic parameters of the radicals detected were obtained from direct measurements of magnetic field and microwave frequency.

3. Results and Discussions

3.1 Photocatalytic activity and photocurrent response

$BiPO_4$ and Bi_2WO_6, as two kinds of Bi^{3+} oxy-acid salt photocatalysts, have been attached great importance by more and more researchers in recent years [8, 11, 18, 22, 29]. $BiPO_4$ possesses superior ultraviolent photocatalytic performance, and Bi_2WO_6 possesses excellent visible activity. Before irradiation, the suspensions of MB over $BiPO_4$, Bi_2WO_6 and $BiPO_4/Bi_2WO_6$ composite photocatalysts were ultrasonically dispersed for 0.5 h and stirred in the dark for 1.0 h to get the adsorption-desorption equilibrium. The initial concentration of MB is 1.0×10^{-5} $mol\cdot L^{-1}$, the initial photocatalytic reaction concentration of MB over $BiPO_4$ and Bi_2WO_6 is 0.98×10^{-5} $mol\cdot L^{-1}$ and 0.85×10^{-5} $mol\cdot L^{-1}$ after reaching the

adsorption-desorption equilibrium (Fig.1), which indicated that Bi_2WO_6 had more adsorption capacity of MB than $BiPO_4$. At the same time, the adsorption capacity of MB over $BiPO_4/Bi_2WO_6$ composite photocatalysts gradually decreased with the content of $BiPO_4$ increasing. The initial photocatalytic reaction concentration of MB over 5.0%$BiPO_4/Bi_2WO_6$ is 0.92×10^{-5} mol·L^{-1}. So the adsorption of MB over photocataysts in this work wouldn't affect greatly the evaluation of photocatalytic performance. Under simulant sunlight irradiation, the photocatlytic activities of $BiPO_4$ and Bi_2WO_6 on the degradation of MB were very low. The apparent rate constant *k* of $BiPO_4$ on the photocatalytic degradation of MB was only 0.0012 min^{-1}, the photocatalytic activity of Bi_2WO_6 on the degradation of MB was higher (k=0.0095min^{-1}) as a visible photocatalyst. $BiPO_4/Bi_2WO_6$ (BPW in Fig) composite photocatalysts possessed better photocatalytic performance on the degradation of MB under simulant sunlight irradiation. When the content of $BiPO_4$ was under 5.0%, the photocatalytic activity of $BiPO_4/Bi_2WO_6$ composites increased gradually with increasing the content of $BiPO_4$. The photocatalytic performance of 5.0%$BiPO_4/Bi_2WO_6$ was the best and its apparent rate constant *k* was 0.0305min^{-1}, which was about 25.4 and 3.2 times of pure $BiPO_4$ and Bi_2WO_6 respectively. When the content of $BiPO_4$ exceeded 5.0%, the photocatalytic activity of $BiPO_4/Bi_2WO_6$ composites decreased gradually with the content of $BiPO_4$ increasing, the above result was accorded with literatures [24, 30, 34, 37]. Because the high content of $BiPO_4$ would reduce the absorption properties of Bi_2WO_6 under simulant sunlight conditions, which further decreased the photocatalytic performance of $BiPO_4/Bi_2WO_6$. The photocatalytic activity of 10%$BiPO_4/Bi_2WO_6$ was lower than that of pure Bi_2WO_6.

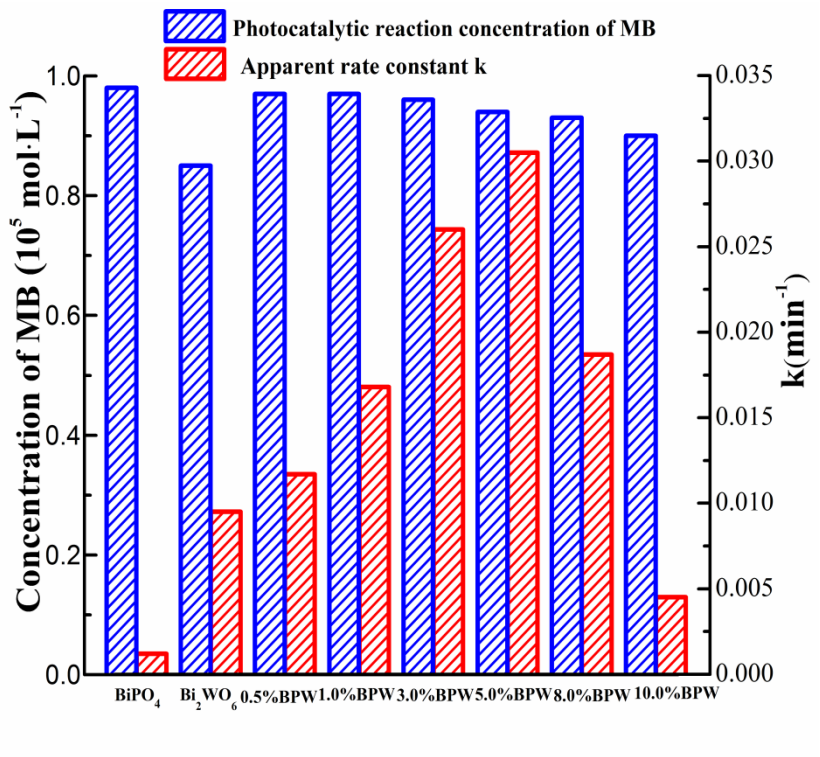

Fig.1 The adsorption and and apparent rate constants of photocatalytic degradation MB over $BiPO_4$, Bi_2WO_6 and $BiPO_4/Bi_2WO_6$ (500W Xenon lamp, [MB]=1.0×10^{-5} mol·L^{-1})

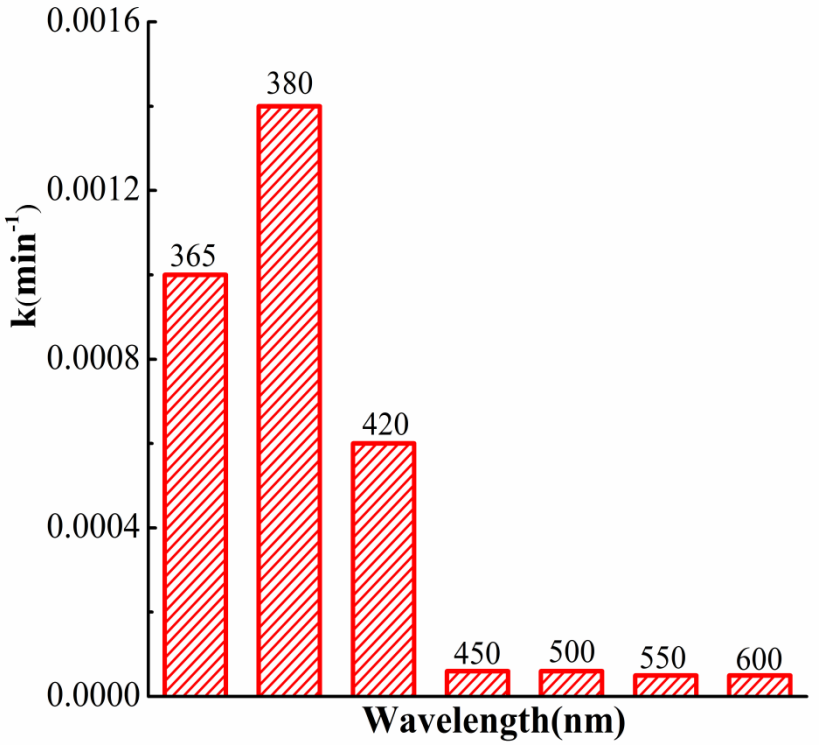

Fig.2 Photocatalytic activity of 5.0%$BiPO_4/Bi_2WO_6$ depended on wavelength

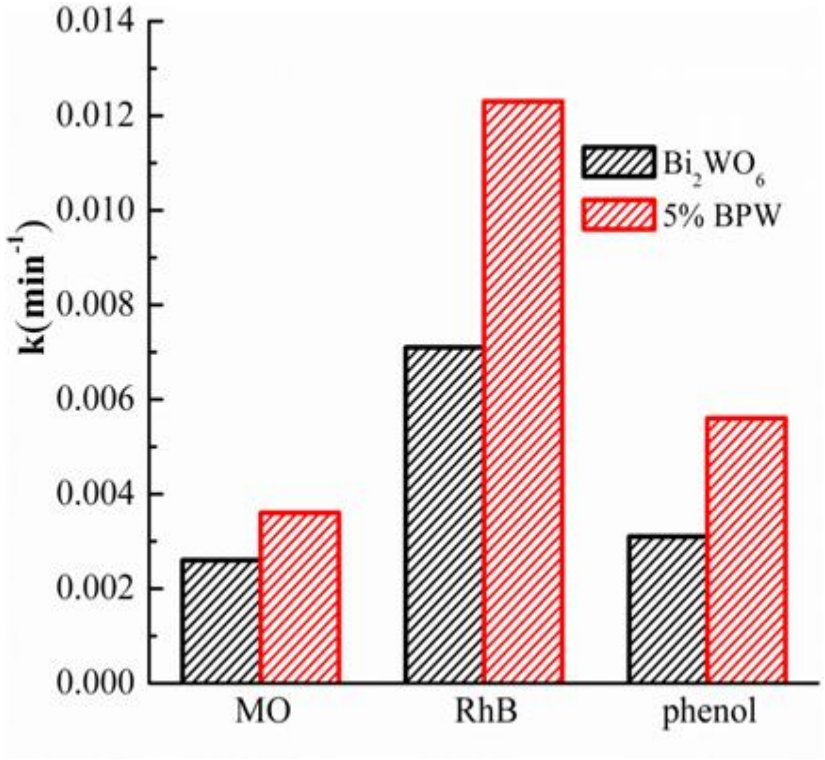

Fig.3 Photocatalytic degradation of different kinds of organic pollutants over Bi_2WO_6 and 5.0%$BiPO_4$/Bi_2WO_6 under simulant sunlight condition (500W Xenon lamp, 25mg photocatalyst, [MO]=1.0×10^{-5} mol·L^{-1}, [RhB]=1.0×10^{-5} mol·L^{-1}, [phenol]=5.0 ppm)

Wavelength dependent photocatalytic activities of 5.0%$BiPO_4$/Bi_2WO_6 were also measured in order to study its light absorption properties and the best excitation wavelength under simulant sunlight irradiation with band-pass filter. As can be seen from Fig. 2, 5.0%$BiPO_4$/Bi_2WO_6 had higher photocatalytic activity at 380 nm than that at 365 nm and 420 nm. Which demonstrated that 380 nm was the best excitation wavelength. With wavelength increasing above 420 nm the photocatalytic performance of 5.0%$BiPO_4$/Bi_2WO_6 were all very low, because long wavelength didn't excite its photo-generated charges.

$BiPO_4$/Bi_2WO_6 composite photocatalysts were investigated to degrade different kinds of organic pollutants popularly. Bi_2WO_6 and 5.0%$BiPO_4$/Bi_2WO_6 were selected to degrade cationic dye MO, anionic dye RhB and neutral colorless reagent phenol under simulant sunlight condition (Fig. 3). 5.0%$BiPO_4$/Bi_2WO_6 exhibited better photocatalytic performance on the degradation of these organic pollutants than pure Bi_2WO_6. The above results showed that $BiPO_4$/Bi_2WO_6 composite photocatalysts had no-selectivity and could effectively degrade different kinds of organic pollutants [26, 41].

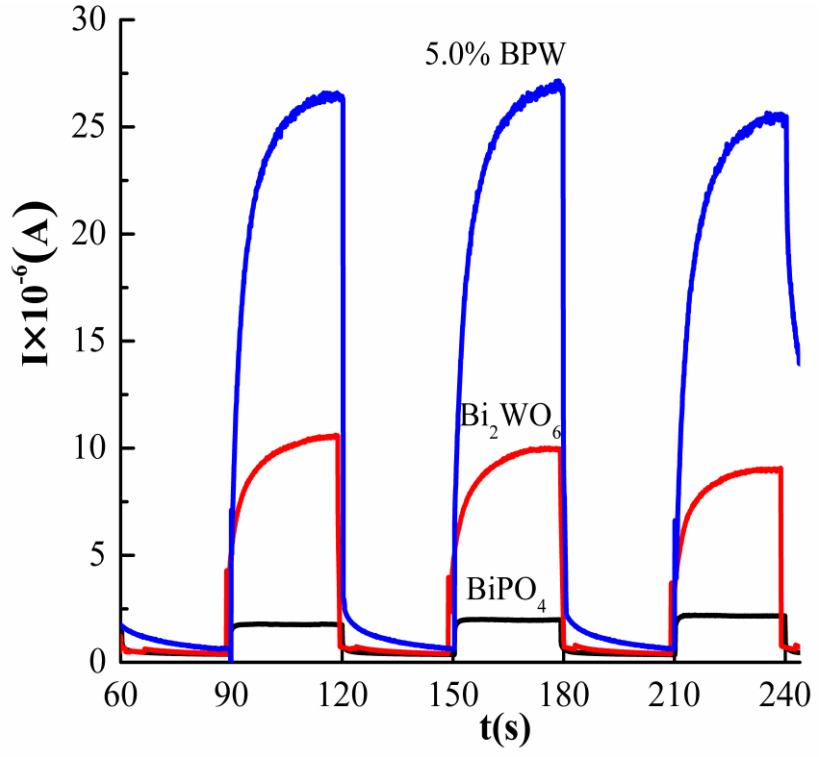

Fig.4 Photocurrent responses of $BiPO_4$, 5.0%$BiPO_4$/Bi_2WO_6 and Bi_2WO_6 under simulant sunlight irradiation

During the photocatalytic process, the separation and transfer of photo-generated charges are the important step that determines photocatalytic efficiency. The photocurrent responses of photocatalyst on the ITO conductive glass under light irradiation could demonstrate the separation and transfer efficiency of photo-generated electrons and holes [42, 43]. The transient photocurrent responses of $BiPO_4$, 5.0%$BiPO_4$/Bi_2WO_6 and Bi_2WO_6 at light-on and light-off were reversible and stable (Fig. 4). Due to a little ultraviolent in the simulant sunlight, the photocurrent response of $BiPO_4$ was very weak. The photocurrent of Bi_2WO_6 was much better than that of $BiPO_4$. The photocurrent of 5.0%$BiPO_4$/Bi_2WO_6 was the highest (26 μA) and about 2.5 times as high as that of pure Bi_2WO_6. The enhancement of photocurrent of 5.0%$BiPO_4$/Bi_2WO_6 composite photocatalyst indicated that the intimate interaction was existed between $BiPO_4$ and Bi_2WO_6 interface, which improved the separation of photo-generated electrons and holes and further enhanced $BiPO_4$/Bi_2WO_6 photocatalytic performance [13, 16, 29, 42].

3.2 Characterization of $BiPO_4$/Bi_2WO_6 composites

As can be seen from the TEM images that precursor $BiPO_4$ was nanorod (Fig. 5a) [25] and pure Bi_2WO_6 was nanosheet (Fig. 5b) [44, 45]. The morphology of 1.0%$BiPO_4$/Bi_2WO_6 composite photocatalyst was the same as that of Bi_2WO_6 nanosheet, there was no big

difference (Fig. 5c). With increasing the content of $BiPO_4$, it can be seen that the core-hole structures of Bi_2WO_6 nanosheet produced around $BiPO_4$ nanorod were gradually formed from the TEM images of $BiPO_4/Bi_2WO_6$ composite photocatalysts (Fig. 5c and f). The TEM image of 5.0%$BiPO_4/Bi_2WO_6$ obviously displayed that core-hole structure of Bi_2WO_6 nanosheet formed around $BiPO_4$ nanrod (Fig. 5e). With the content of $BiPO_4$ further increasing, the TEM image of 8.0% $BiPO_4/Bi_2WO_6$ showed a part of bare $BiPO_4$ nanorod (Fig. 5f). It was indicated that too much content of $BiPO_4$ would destroy the core-hole structure of $BiPO_4/Bi_2WO_6$ composite photocatalysts and further decreased its absorption efficiency and photocatalytic performance.

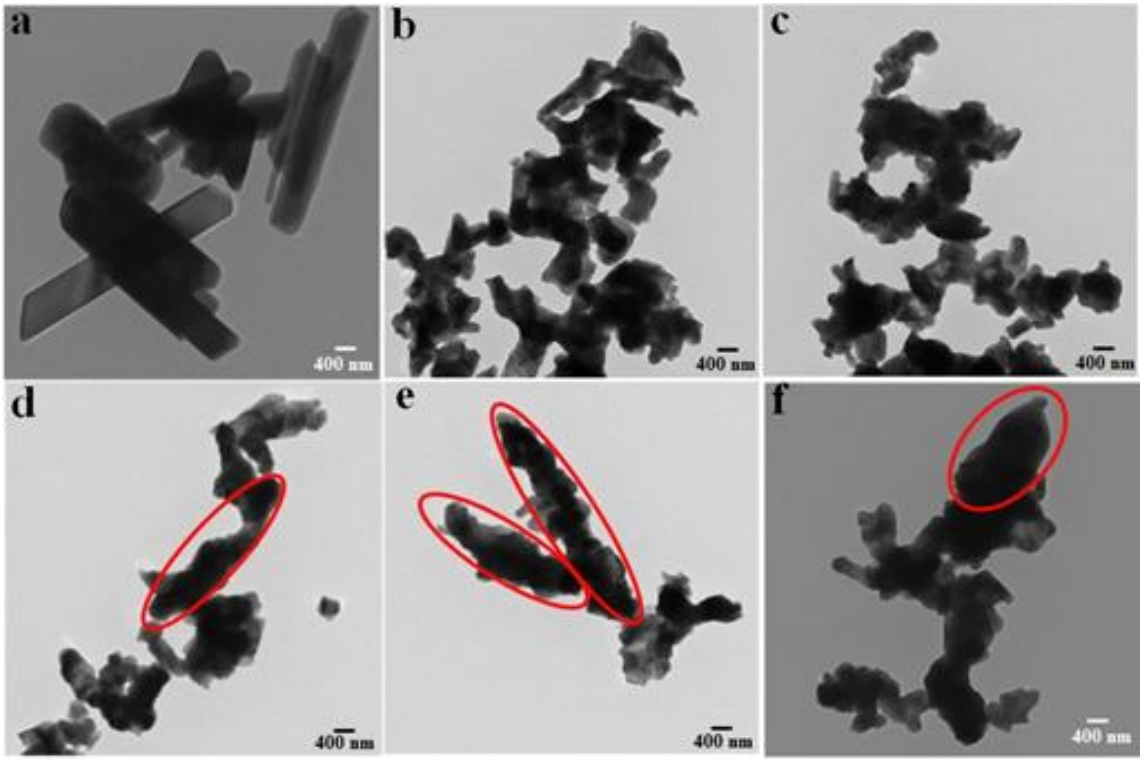

Fig.5 The TEM images of $BiPO_4$, $BiPO_4/Bi_2WO_6$ composites and Bi_2WO_6

（a, $BiPO_4$; b, Bi_2WO_6; c, 1.0%$BiPO_4/Bi_2WO_6$; d 3.0%$BiPO_4/Bi_2WO_6$; e, 5.0%$BiPO_4/Bi_2WO_6$; f, 8.0%$BiPO_4/Bi_2WO_6$）

The core-hole structure of $BiPO_4/Bi_2WO_6$ was further demonstrated by the EDS mapping and HRTEM images (Fig.6 and Fig.7). The elemental composition and mapping of 5.0%$BiPO_4/Bi_2WO_6$ were examined by EDS mapping (Fig.6). Bi, P, W, O elements were all existed in 5.0%$BiPO_4/Bi_2WO_6$ composite photocatalyst. P element distributed the main body of $BiPO_4$ nanorod, but W element distributed the margin of $BiPO_4$ nanrod and a part of W elements were enriched on the surface of $BiPO_4$ nanrod. The Fig.7a was the HRTEM image of Bi_2WO_6, the lattice fringes of 0.193 nm, 0.273 nm and 0.318 nm belonged to the lattice plane

of Bi_2WO_6 orthorhombic (JPCDS 079-2381) (202), (002) and (131). From the HRTEM image of 5.0%$BiPO_4$/Bi_2WO_6, the (200) lattice plane of $BiPO_4$ about 0.330 nm lattice dispace ascribed to monazite monoclinic (JPCDS 089-0287) was coated by the (002) and (131) lattice plane of Bi_2WO_6. Moreover, the heterojunction was formed between the (002), (131) lattice plane of Bi_2WO_6 and the (200) lattice plane of $BiPO_4$.

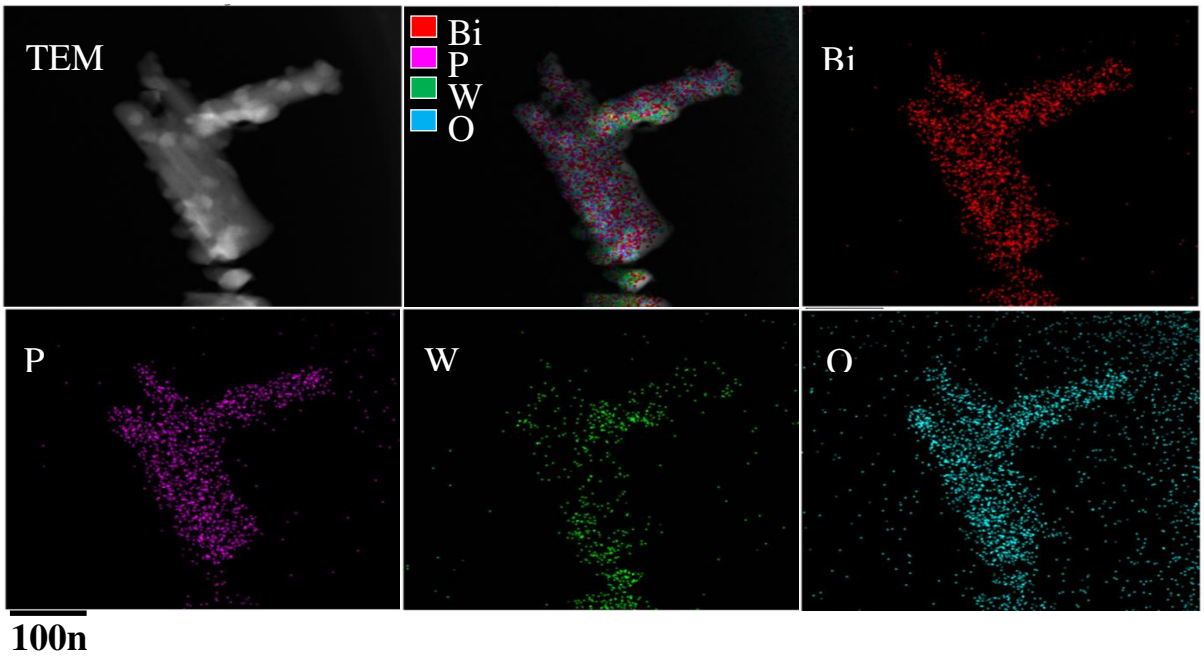

Fig.6 The EDS mapping of 5.0%$BiPO_4$/Bi_2WO_6

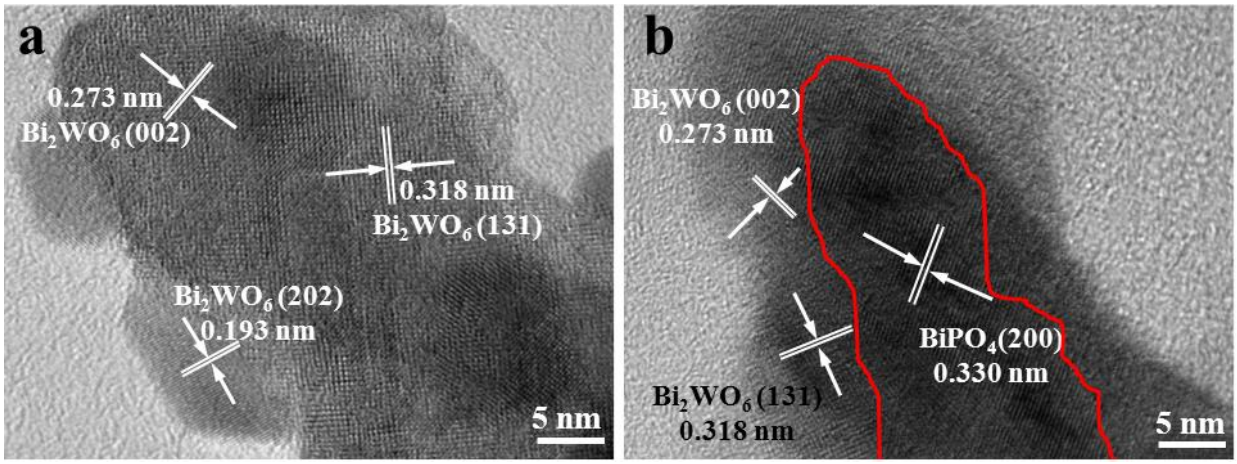

Fig.87 HRTEM images of Bi_2WO_6 (a) and 5.0%$BiPO_4$/Bi_2WO_6 (b)

In order to investigate the valance bond interaction between $BiPO_4$ and Bi_2WO_6 in $BiPO_4$/Bi_2WO_6 composite photocatalysts, the characteristic Raman spectra of samples were tested. Bi_2WO_6 has five characteristic Raman spectra, which located in 826 cm^{-1}, 792 cm^{-1}, 718 cm^{-1}, 433 cm^{-1} and 298 cm^{-1} respectively(Fig.8). 826 cm^{-1} and 792 cm^{-1} were ascribed to the symmetric and anti-symmetric stretching modes of terminal O-W-O, the peak of 718 cm^{-1}

was anti-symmetric bridging mode associated with the tungstate chain. Moreover, the peak of 433 cm^{-1} was ascribed to anti-symmetric mode of WO_6 octahedral, the Raman peak of 298 cm^{-1} was assigned to translational modes of simultaneous motions of Bi^{3+} and WO_6^{6-}[46-48]. The Raman spectrum of 5.0%$BiPO_4$/Bi_2WO_6 included the all characteristic peaks of Bi_2WO_6. Among them, the 298 cm^{-1} peak of Bi_2WO_6 produced a red shift to 301 cm^{-1}, but the peaks located at 826 cm^{-1}, 792 cm^{-1}, 718cm^{-1} produced a little blue shift. It was indicated that $BiPO_4$ changed the chemical bond energy of Bi_2WO_6 in the $BiPO_4$/Bi_2WO_6 composite photocatalysts. There was chemical bond interaction between $BiPO_4$ and Bi_2WO_6. Moreover, the characteristic Raman peaks of $BiPO_4$ located at 414cm^{-1}, 572cm^{-1}, 1006cm^{-1} and 1079 cm^{-1} appeared in the Raman peaks of 5.0%$BiPO_4$/Bi_2WO_6 [26]. The composite of $BiPO_4$/Bi_2WO_6 didn't change the crystal structure of $BiPO_4$ and Bi_2WO_6, and the all characteristic peaks of Bi_2WO_6 orthorhombic (JPCDS 079-2381) appeared. With increasing the content of $BiPO_4$, the characteristic peaks of its monazite monoclinic (JPCDS 089-0287） were gradually demonstrated (Fig. S1).

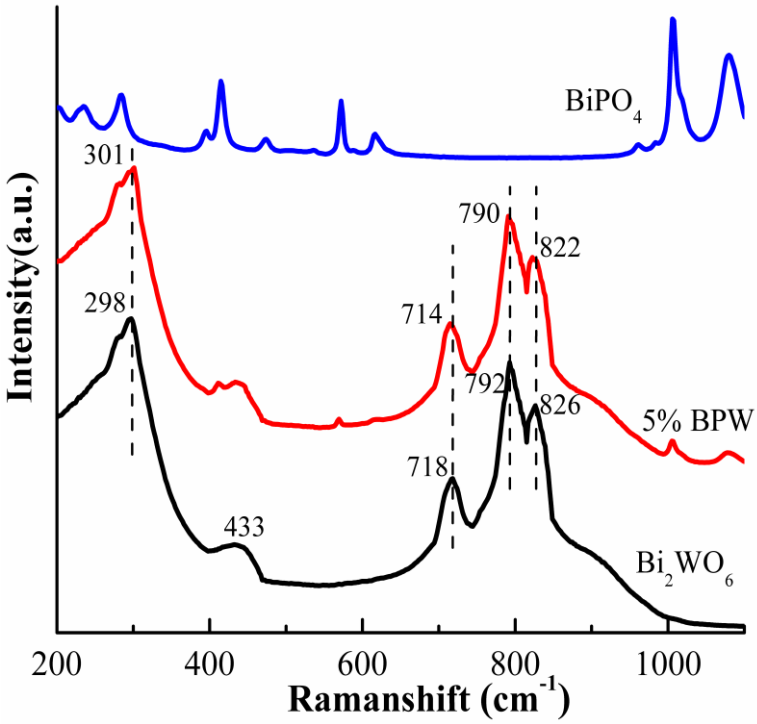

Fig.8 Raman spectra of Bi_2WO_6, 5.0%$BiPO_4$/Bi_2WO_6 and $BiPO_4$

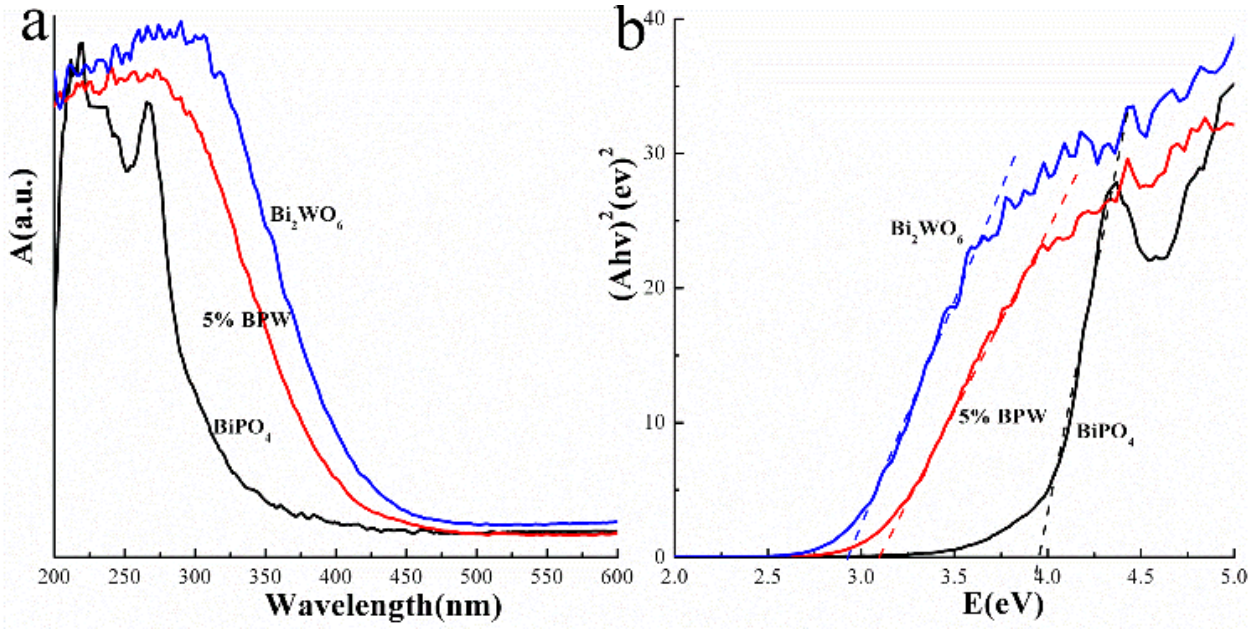

Fig.9 UV-Vis spectra of Bi_2WO_6, 5.0%$BiPO_4$/Bi_2WO_6 and $BiPO_4$

The UV-Vis spectra of $BiPO_4$, Bi_2WO_6 and 5.0%$BiPO_4$/Bi_2WO_6 were showed in Fig. 9. The absorption band edge of precursor $BiPO_4$ was about 320 nm (Fig. 9a) [25]。 Bi_2WO_6, as a visible photocatalyst, its absorption band edge was about 460 nm. In the range of 200-450 nm, the strong absorption of Bi_2WO_6 ascribed to the charge transfer from O^{2-} to W^{6+}[4, 10]. The absorption band edge of 5.0%$BiPO_4$/Bi_2WO_6 composite photocatalyst was about 385 nm, which induced an obvious red shift compared to $BiPO_4$ and a blue shift compared to Bi_2WO_6. The above results illustrated that there was chemical interaction between Bi_2WO_6 and $BiPO_4$ interface, which improved the separation and transfer of photo-generated charges. According to the calculated Tauc's plot, the band gaps of Bi_2WO_6, 5.0%$BiPO_4$/Bi_2WO_6 and $BiPO_4$ were 2.7 eV, 3.2 eV and 3.9 eV respectively (Fig. 9b).

3.3 Proposed enhancement mechanism of $BiPO_4$/Bi_2WO_6 photocatalytic activity

The separation of photo-generated electrons and holes played a very important role during the photocatalytic process of decomposition of organic pollutants, which could be evaluated by the typical electrochemical impedance spectra (EIS)[21, 26, 29, 41]. Under simulant sunlight irradiation and in dark, The EIS Nyquist plots of $BiPO_4$, Bi_2WO_6 and 5.0%$BiPO_4$/Bi_2WO_6 were presented in Fig. 10. The arc radius on the EIS spectra reflects the solid state interface layered resistance and the surface charges transfer resistance. The smaller arc radius on the EIS Nyquist plot indicates a more efficient separation of the photo-generated electrons and holes, and vice versa. The Nyquist arc radii of 5.0%$BiPO_4$/Bi_2WO_6 were all smaller than that of $BiPO_4$ and Bi_2WO_6, which illustrated that $BiPO_4$/Bi_2WO_6 composite photocatalyst had smaller electric resistance and higher efficiency

of charges separation than $BiPO_4$ and Bi_2WO_6. Thus, 5.0%$BiPO_4$/Bi_2WO_6 photocatalyst has higher separation efficiency of photo-generated charges and better photocatalytic activity.

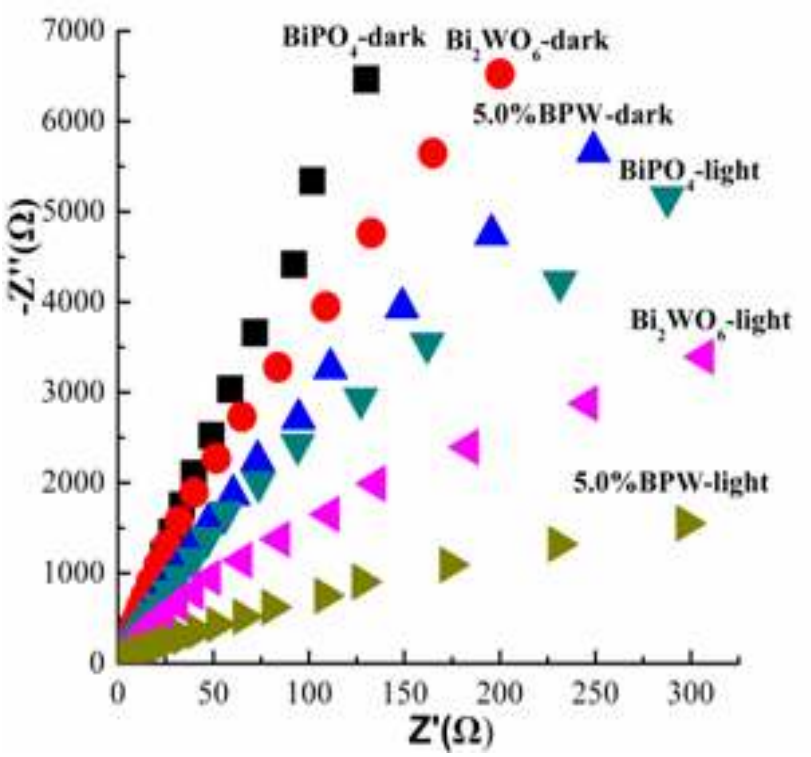

Fig.-10 The EIS response of Bi_2WO_6, 5.0%$BiPO_4$/Bi_2WO_6 and $BiPO_4$ thin film electrodes in dark and under simulant sunlight irradiation

The main oxidative species of semiconductor photocatalysts could be verified by the trapping experiments of active species, usually using ethylenediamine tetraacetic acid disodium salt (EDTA-2Na) as hole scavengers, tertiary butyl alcohol (t-BuOH) as hydroxyl radical scavengers and purging N_2 as $\cdot O^{2-}$ radical scavenger. The oxidative species on the photocatalytic degradation of MB over Bi_2WO_6 and 5.0%$BiPO_4$/Bi_2WO_6 were shown in Fig. 11. When the N_2 was purged the photocatalytic activity of Bi_2WO_6 and 5.0% $BiPO_4$/Bi_2WO_6 didn't changed, which indicated that $\cdot O^{2-}$ radical wasn't the main oxidative species. The photocatalytic performance of Bi_2WO_6 and 5.0%$BiPO_4$/Bi_2WO_6 changed slightly by addition of t-BuOH, suggesting that ·OH radical played an assistant role on the photocatalytic degradation of MB over Bi_2WO_6 and 5.0%$BiPO_4$/Bi_2WO_6. Moreover, the ESR spin-trap technique was used to monitor the oxidative species generated by Bi_2WO_6 and 5.0%$BiPO_4$/Bi_2WO_6 with DMPO in water and Methyl alcohol under light irradiation (Fig. S2). The result of ESR further demonstrated that there was no $\cdot O^{2-}$ radical in the system of Bi_2WO_6 and 5.0%$BiPO_4$/Bi_2WO_6. However, the intensity of ·OH radical in 5.0%$BiPO_4$/Bi_2WO_6 system was much higher than that of Bi_2WO_6. The photocatalytic

activity of Bi_2WO_6 and 5.0%$BiPO_4/Bi_2WO_6$ decreased greatly by addition of EDTA-2Na, which improved that photo-generated holes are the main oxidative species of Bi_2WO_6 and 5.0%$BiPO_4/Bi_2WO_6$.

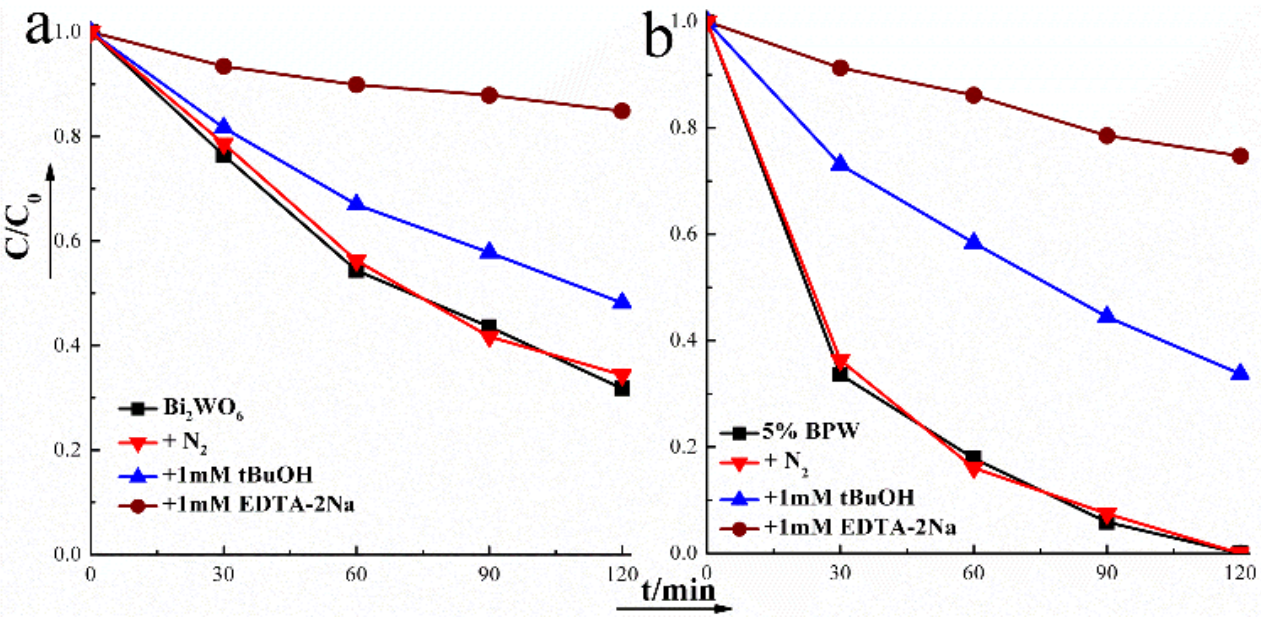

Fig.~~10~~11 The plots of photocatalytic degradation of MB over Bi_2WO_6（a）and 5.0%$BiPO_4/Bi_2WO_6$ (b) with the addition of hole, $\cdot O^{2-}$ and ·OH radical scavenger under simulant sunlight irradiation

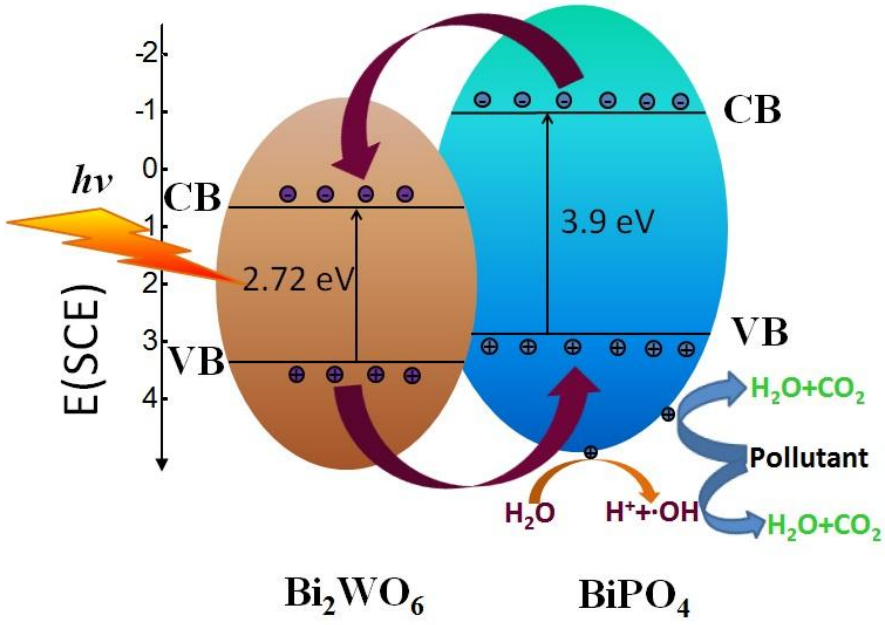

Fig.12 The proposed mechanism of charges separation and enhancement of $BiPO_4/Bi_2WO_6$ photocatalytic activity

Based on the above results, a proposed enhancement mechanism of charges separation and photocatalytic process over $BiPO_4/Bi_2WO_6$ was inferred in Fig.12. During the photocatalytic process of $BiPO_4/Bi_2WO_6$ composites under simulant sunlight

irradiation, Bi_2WO_6 could absorb visible light to form photo-generated holes that transited to the valance band of $BiPO_4$, at the same time $BiPO_4$ could absorb ultraviolet to form photo-generated electrons that transited to the conduction band of Bi_2WO_6. The interaction of $BiPO_4$ and Bi_2WO_6 not only expanded the range of absorption spectrum but also enhanced the separation and transfer efficiency of photo-generated charges, and then further improving the photocatalytic performance. According to the result of main oxidative species detection, the photo-generated holes of $BiPO_4$ valance band could degrade the organic pollutants directly or react with water to form ·OH radical that further decompose organic pollutants.

4. Conclusions

In this work, $BiPO_4/Bi_2WO_6$ composite photocatalysts were prepared via ultrasonic-calcination method. Compared with pure $BiPO_4$ and Bi_2WO_6, $BiPO_4/Bi_2WO_6$ has superior photocatalytic performance for degrading different kinds of organic pollutants under simulant sunlight irradiation. In the $BiPO_4/Bi_2WO_6$ composite photocatalysts, the core-hole structure of $BiPO_4$ as core and Bi_2WO_6 as hole was formed. The photo-generated electrons of $BiPO_4$ would inject to conduction band of Bi_2WO_6, and the photo-generated holes on Bi_2WO_6 could transfer to the valance band of $BiPO_4$, and then an effective charges separation was achieved. The interaction of $BiPO_4$ and Bi_2WO_6 not only expanded the range of absorption spectrum but also enhance the separation efficiency of photo-generated charges, which then improve the photocatalytic performance.

Acknowledgements

This work was partly supported by National Basic Research Program of China (2013CB632403) and Chinese National Science Foundation (21437003and 21307020).

References

[1] A. Tang, Y. Jia, S. Zhang, Q. Yu, X. Zhang, Catalysis Communications 50 (2014) 1-4.
[2] D. Spasiano, R. Marotta, Appl. Catal. B: Environ. 170-171 (2015) 90-123.
[3] R.a. He, S. Cao, P. Zhou, J. Yu, Chinese Journal of Catalysis 35 (2014) 989-1007.
[4] Y. Liu, H. Lv, J. Hu, Z. Li, Materials Letters 139 (2015) 401-404.
[5] S. Hu, C. Xu, W. Wang, F. Ma, L. Zhen, Ceramics International 40 (2014) 11689-11698.
[6] K. Akihiko, s. Hijii, Chemisty Letters 28 (1999) 1103-1104.
[7] X. Chu, G. Shan, C. Chang, Y. Fu, L. Yue, L. Zhu, Front. Environ. Sci. Eng. 10 (2016) 211-218.

[8] J. Liu, Y. Bai, P. Wang, Micro & Nano Letters 8 (2013) 90-93.
[9] J. Lin, Z. Guo, Z. Zhu, Ceramics International 40 (2014) 6495-6501.
[10] Z. Zhang, W. Wang, E. Gao, S. Sun, L. Zhang, J. Phys. Chem. C 116 (2012) 25898-25903.
[11] R.M. Mohameda, E.S. Aazam, Materials Research Bulletin 48 (2013) 3572-3578.
[12] J. Zhang, Z. Huang, Y. Xu, F. Kang, International Journal of Photoenergy (2012).
[13] M. Shang, W. Wang, L. Zhang, S. Sun, L. Wang, L. Zhou, J. Phys. Chem. C 113 (2009) 14727-14731.
[14] X. Liu, Q. Lu, J. Liu, Journal of Alloys and Compounds 662 (2016) 598-606.
[15] D. Wang, L. Guo, Y. Zhen, L. Yue, G. Xue, F. Fu, J. Mater. Chem. A 2 (2014) 11716-11727.
[16] G. Fu, G. Xu, S. Chen, L. Lei, M. Zhang, Catal. Commun. 40 (2013) 120-124.
[17] S. Xue, Z. Wei, X. Hou, W. Xie, S. Li, X. Shang, D. He, Applied Surface Science 355 (2015) 1107-1115.
[18] M. Gui, W. Zhang, Q. Su, C. Chen, Journal of Solid State Chemistry 184 (2011) 1977-1982.
[19] Q. Xiao, J. Zhang, C. Xiao, X. Tan, Catal. Commun. 9 (2008) 1247-1253.
[20] M. Li, L. Zhang, X. Fan, Y. Zhou, M. Wu, J. Shi, J. Mater. Chem. A 3 (2015) 5189-5196.
[21] Y. Wang, X. Bai, C. Pan, J. He, Y. Zhu, J. Mater. Chem. 22(23) (2012) 11568-11573.
[22] C. Pan, D. Li, X. Ma, Y. Chen, Y. Zhu, Catal. Sci. Technol. 1 (2011) 1399-1405.
[23] C. Pan, Y. Zhu, Environ. Sci. Technol. 44 (2010) 5570-5574.
[24] C. Pan, Y. Zhu, Catal. Sci. Technol. 5 (2015) 3071-3083.
[25] Y. Zhu, Y. Liu, Q. Ling, Y. Lv, H. Wang, Y. Zhu, Acta Phys. -Chim. Sin. 29 (2013) 576-584.
[26] Y. Zhu, Y. Liu, Y. Lv, Q. Ling, D. Liu, Y. Zhu, J. Mater. Chem. A 2 (2014) 13041-13048.
[27] J. Qian, Z. Yang, C. Wang, K. Wang, Q. Liu, D. Jiang, Y. Yan, K. Wang, J. Mater. Chem. A 3 (2015).
[28] Z. Li, S. Yang, J. Zhou, D. Li, X. Zhou, C. Ge, Y. Fang, Chemical Engineering Journal 241 (2014) 344-351.
[29] C. Pan, J. Xu, Y. Wang, D. Li, Y. Zhu, Adv. Funct. Mater. 22 (2012) 1518-1524.
[30] Y. Liu, W. Yao, D. Liu, R. Zong, M. Zhang, X. Ma, Y. Zhu, Appl. Catal. B: Environ. 163 (2015) 547-553.
[31] J. Cao, B. Xu, H. Lin, S. Chen, Chemical Engineering Journal 228 (2013) 482-488.
[32] W. An, W. Cui, Y. Liang, J. Hu, L. Liu, Applied Surface Science 351 (2015) 1131-1139.
[33] F. Duo, C. Fan, Y. Wang, Y. Cao, X. Zhang, Materials Science in Semiconductor Processing 38 (2015) 157-164.
[34] S. Wu, H. Zhengn, Y. Wu, W. Lin, T. Xu, M. Guan, Ceramics International 40 (2014) 14613-14620.
[35] N. Mohaghegh, E. Rahimi, M.R. Gholami, Materials Science in Semiconductor Processing 39 (2015) 506-514.
[36] N. Mohaghegh, M. Tasviri, E. Rahimi, M.R. Gholami, Applied Surface Science 351 (2015) 216-224.
[37] X. Lin, D. Liu, X. Guo, N. Sun, S. Zhao, L. Chang, H. Zhai, Q. Wang, Journal of Physics and Chemistry of Solids 76 (2015) 170-177.
[38] S. Ganguli, C. Hazra, M. Chatti, T. Samanta, Langmuir 32 (2016) 247-253.
[39] H. Xu, Y. Xu, H. Li, J. Xia, J. Xiong, S. Yin, C. Huang, H. Wan, Dalton Transactions 41 (2012) 3387-3394.
[40] H. Ye, H. Lin, J. Cao, S. Chen, Y. Chen, Journal of Molecular Catalysis A: Chemical 397 (2015) 85-92.
[41] Y. Lv, Y. Zhu, Y. Zhu, J. Phys. Chem. C 117 (2013) 18520-18528.
[42] H. Huang, L. Liu, Y. Zhang , N. Tian, Journal of Alloys and Compounds 619 (2015) 807-811.
[43] Z. Pei, S. Weng, P. Liu, Appl. Catal. B: Environ. 180 (2016) 463-470.
[44] L. Zhou, W. Wang, L. Zhang, Journal of Molecular Catalysis A: Chemical 268 (2007) 195-200.
[45] F. Zhang, F. Xie, J. Liu, W. Zhao, K. Zhang, Ultrason. Sonochem. 20 (2013) 209-215.
[46] M. Ge, L. Liu, Materials Science in Semiconductor Processing 25 (2014) 258-263.
[47] A. Phuruangrat, P. Dumrongrojthanath, N. Ekthammathat, S. Thongtem, T. Thongtem, Journal of Nanomaterials 36 (2014) 1-7.

[48] R. Shi, G. Huang, J. Lin, Y. Zhu J. Phys. Chem. C 113 (2009) 19633-19638.

*Graphical Abstract